RSC Advances

COMMUNICATION

View Article Online
View Journal | View Issue

Cite this: *RSC Adv.*, 2014, **4**, 59977

Received 9th October 2014
Accepted 3rd November 2014

DOI: 10.1039/c4ra12029a

www.rsc.org/advances

Recyclable catalyst for catalytic hydrogenation of phenylacetylene by coupling Pd nanoparticles with highly compressible graphene aerogels†

Xu Zhang,[a] Zhiyu Wang,*[a] Shuang Li,[ab] Chunlei Wang[a] and Jieshan Qiu*[a]

Highly compressible 3D graphene aerogels have been fabricated by chemical reduction of graphene oxide with hydroiodic acid at low temperature. They serve as ideal supports to anchor Pd nanoparticles, exhibiting high activity and selectivity with good recyclability towards selective semi-hydrogenation of phenylacetylene to styrene in solution.

Carbon aerogels (CAs), being one of the most important aerogels, have received considerable attention due to their great potential in many fields such as the catalysis,[1,2] energy storage,[3,4] and heavy metal ion removal.[5,6] Specifically, graphene, a single-atom thick sheet of hexagonally arrayed sp^2-bonded carbon atoms, is very appealing building block for the CAs with extraordinary physiochemical properties.[7,8] For example, 3D graphene aerogels (denoted as GAs) have been constructed from the graphene by various approaches such as hydrothermal-mediated assembly,[2,9] chemical reduction,[10,11] electrochemical synthesis,[12] "breath figure" method[13] and template-directed chemical vapor deposition.[14] Most recently, we also developed an efficient strategy for the fabrication of ultralight graphene aerogels by combining the EDA-mediated assembly of the graphene and microwave irradiation technique.[15] However, the practical application of the GAs, especially in catalysis, is still far behind the enormous success in their synthesis perhaps because the structural stability of most GAs is too poor to withstand the catalyst loading and recycled use.

Catalytic hydrogenation, for example, the production of anilines from nitroarenes,[16] is among the most important and widely accessed transformations in industry.[17] In this process, selective semi-hydrogenation of the phenylacetylene to styrene in liquid phase has received particular importance because the formation of phenylacetylene may poison the catalyst for styrene polymerization and reduce the purity of final products.[18] Pd has been recognized as the most efficient catalyst for catalytic hydrogenation of styrene due to the high activity and selectivity.[19] Commonly, Pd nanoparticles are dispersed on the powder-like supports to reduce the processing cost and prevent the products from metal contamination, which however makes the catalyst hardly to be recycled.[20] In this work, we report the facile synthesis of 3D GAs with the assistance of HI in aqueous solution at low temperature. They are very appealing matrix material to support Pd nanoparticles in virtue of several structural merits: (i) as an easily-handled bulk material, 3D GAs can be readily separated from liquid phase for recycle use. The compressible feature further allows Pd/GAs catalyst to be facilely regenerated for many cycles by simply squeezing the residues out, which greatly reduced the process cost and complexity; (ii) the rich porosity of the GAs provides sufficient surface area and interconnected 3D channels, facilitating homogenous dispersion of Pd nanoparticles and diffusion kinetics of catalytic reaction; (iii) the GAs are highly compressible with robust structure, rendering excellent structural stability for catalyst loading and reuse. After loading with ultrafine Pd nanoparticles, the resultant Pd/GAs composite can be directly used as a free-standing, recyclable catalyst for efficiently selective semi-hydrogenation of phenylacetylene.

The synthetic strategy of the GAs is shown in Fig. 1a. GO is firstly dispersed in an aqueous solution of HI to form a gelatinous suspension. The presence of the HI accelerates the ring-opening reaction of the oxygen-containing groups on GO surface.[20] The removal of these groups reduces electrically insulating GO to graphene with restored conjugation. In this process, the hydrophobicity and conjugated structures of graphene are gradually enhanced to facilitate the π–π stacking and cross-linkage of individual graphene sheets; whereas the presence of the I^{3-} and residual oxygenated functional groups in the

[a]*Carbon Research Laboratory, Liaoning Key Lab for Energy Materials and Chemical Engineering, State Key Lab of Fine Chemicals, Dalian University of Technology, Dalian 116024, P. R. China. E-mail: jqiu@dlut.edu.cn; zywang@dlut.edu.cn; Fax: +86-411-84986080; Tel: +86-411-84986024*

[b]*School of Chemical Engineering, Northwest University, Xi'an, Shaanxi 710069, China*

† Electronic supplementary information (ESI) available: Detailed experimental procedures, Raman, XRD, XPS, stress–strain curves and optical image of GAs and Pd/GAs catalyst. See DOI: 10.1039/c4ra12029a

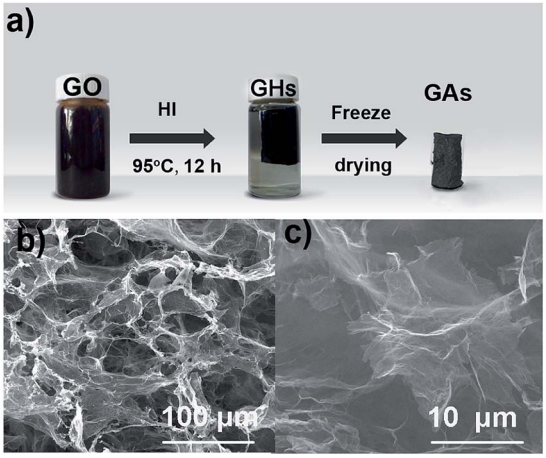

Fig. 1 (a) Synthetic procedure and (b and c) SEM images of the GAs.

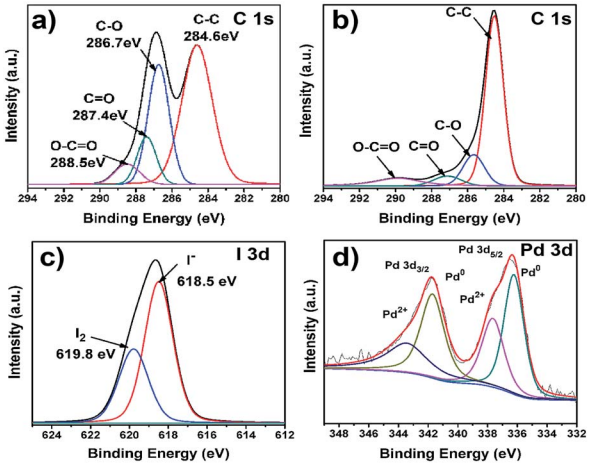

Fig. 2 C 1s XPS spectra of (a) GO and (b) GAs; (c) I 3d spectra of GAs; (d) Pd 3d spectra of Pd/GAs catalyst.

interspace of graphene avoid the complete aggregation of graphene sheets. As a result, cylinder shaped graphene hydrogels are formed by the assembly of the graphene after the reaction for 12 h. After freeze drying, the residual water in graphene hydrogels is carefully removed to avoid the damage of the porosity, eventually yielding well-defined GAs with cylinder shape and high stability in air.

The morphology and microstructure of the GAs is characterized by scanning electron microscopy (SEM), as shown in Fig. 1b and c. It reveals that the GAs posse a foam-like structure with highly developed interconnected 3D channels ranging from tens to hundreds of micrometers. The channel walls are made up of assembled graphene sheets produced during the freezing process where individual sheets are pushed together with the formation of ice crystals and the in-plane size of these assembled sheets can be up to tens of micrometers. Raman spectra of the GAs exhibit two distinctive bands at 1340 cm^{-1} and 1587 cm^{-1}, corresponding to the vibrations of sp^3 carbon atoms of defects, namely the disorder band (D band), and the first-order scattering of the E_{2g} mode for sp^2 carbon lattice (G band), respectively (Fig. S1a†).[21] The intensity ratio of the D and G bands (I_D/I_G) is 1.43, while the corresponding value the GO is as low as 0.91. The increased I_D/I_G value with the restoration of the sp^2 lattice is due to the decrease size of sp^2 domains by the reduction of the GO with HI.[22] The efficient reduction of the GO is also evidenced by XRD analysis, as characterized by the disappearance of the fingerprint peak of the GO at 10.5°, as shown in Fig. S1b.†

X-ray photoelectron spectroscopy (XPS) is employed to detect the variation of elemental composition and functional groups in the samples, as shown in Fig. 2 and S2.† In C 1s spectra, the intensity of the peak corresponding to sp^2-hybridized carbon (at 284.6 eV) increases continually from GO to GAs, while the change of oxygen signals (286.7 eV for C–O, 287.4 eV for C=O and 288.5 eV for O–C=O group) is in opposite trend (Fig. 2a–c).[23] This observation is consistent with the XRD and Raman results, revealing the partial restoration of the conjugated graphene sheets *via* effective removal of oxygen-containing groups from GO. The presence of residual iodine in GAs is shown as the peak at 619.8 and 618.5 eV for the neutral iodine and the iodine anion in Fig. 2d, respectively.[23] Nitrogen adsorption test shows that the specific surface area of the GAs is 84 $m^2\ g^{-1}$ (Fig. S3†).

Structural stability of the supports represents a very important issue for the construction of durable catalyst. The GAs exhibit excellent mechanical stability, especially high compressibility against fatigue cyclic compression with a strain up to 50% at a high loading rate of 60 mm min^{-1} (the test device is shown in Fig. S4†). The compressive strain (ε) curve of the first cycle depicts two distinct stages during the loading process, the linear-elastic regime ($\varepsilon < 15\%$) and the non-linear regime ($15\% < \varepsilon < 50\%$). The initial compression cycle shows higher Young's modulus (3 kPa) and maximum stress (6.3 kPa). From the 10th cycle onwards, the Young's modulus and maximum stress of GAs at $\varepsilon = 50\%$ keep nearly unchanged. After compressed for 100 cycles, the volume of the GAs remains almost the same without a discernible variation or cracking compared to the original morphology, retaining 81% of the maximum stress with 14% of compressive strain lost. Apparently, this structure could allow a large deformation without fracture or collapse, being highly durable matrix to support the catalyst particles.

The robust structure of the GAs provides the feasibility for uniform dispersion of Pd nanoparticles by the impregnation of GAs in ethanol solution of Na_2PdCl_4, followed by annealing and reduction by H_2 at 100 °C. Transmission electron microscopy (TEM) characterization indicates the homogenous dispersion of Pd nanoparticles with an average size of 3.8 nm on GAs (Fig. 3a and b and S5†). Despite the small size, Pd nanoparticles retain the single crystalline structure with clear lattice fringe from (111) plane of Pd crystal ($d_{111} = 0.225$ nm).[24] Elemental mapping further confirms the uniform distribution of Pd nanoparticles on Gas surface, as shown in Fig. 3f. In XRD pattern of Pd/GAs catalyst, all the diffraction peaks can be assigned to (111) and (200) reflections of Pd (JCPDS no. 46-1043) except the broad peak from the graphene at 26° (Fig. S2b†). The peak corresponds to the (311) plane of Pd is too weak to be detected due to

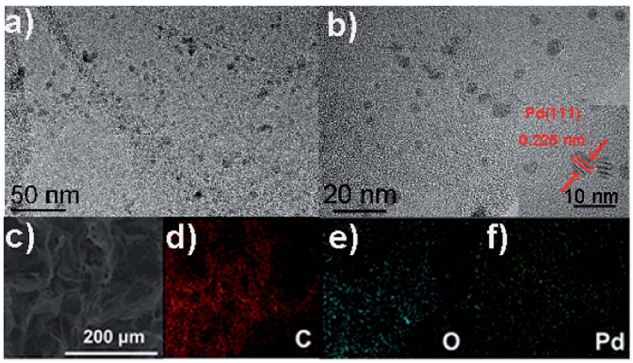

Fig. 3 (a and b) TEM images of Pd/GAs catalyst; (c) SEM image of Pd/GAs catalyst; (d–f) elemental mapping showing the homogenous distribution of C, O and Pd in the catalyst, respectively.

the extremely small size of Pd particles.[24] XPS analysis also indicates the presence of Pd element, as shown in Fig. 2d. Two peaks are observed at 336.2 eV and 341.7 eV that can be assigned to Pd $3d_{5/2}$ and Pd $3d_{3/2}$ doublet, respectively.[25] Overall, the loading amount of the Pd is 6.7 wt%, as determined by ICP analysis.

The catalytic performance of Pd/GAs catalyst is evaluated with selective semi-hydrogenation of phenylacetylene as a probe reaction (Scheme S2†). On the first run, the conversion of phenylacetylene in solvent is 75.0% with a high selectivity of 97.0%, as shown in Fig. 4. After the reaction, Pd/GAs catalyst is separated from the liquid phase by the tweezers and is squeezed to discharge the residual products adsorbed on the catalyst. The leaching of Pd in the solvent is not detected by ICP analysis, namely, the hydrogenation over Pd/GAs catalyst is basically a heterogeneous process. After thoroughly rinsing with ethanol, the activity of Pd/GAs catalyst can be increased to 87.3% on the second run due to the swelling effect that improves the diffusion of phenylacetylene in highly porous catalyst.[26] After the sixth run, the conversion of phenylacetylene can be as high as 83.0% with a high selectivity of 97.9%. For each run, the reaction yield of phenylethylene is 72.8%, 84.6%, 87.8%, 82.8%, 88.6% and 81.3%, respectively. The post-mortem study shows that the original properties of Pd/GAs catalyst can be well retained in terms of the shape, size and structural integrity, indicating the excellent structural stability of this material (Fig. S6†). Without using the catalyst, however, no reaction occurs in the blank test due to the absence of Pd nanoparticles. Apparently, Pd/GAs catalyst has demonstrated excellent catalytic properties and good recyclability towards selective semi-hydrogenation reaction of phenylacetylene.

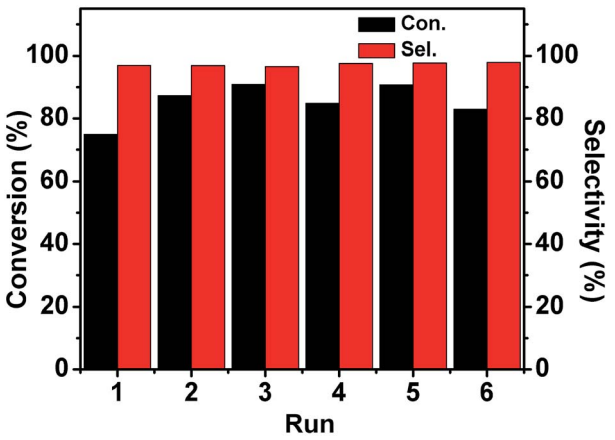

Fig. 4 Recyclability of Pd/GAs catalyst towards catalytic hydrogenation of phenylacetylene.

Conclusions

In summary, highly compressible GAs have been fabricated *via* HI-mediate chemical reduction of GO at low temperature, followed by freezing–drying. They feature with easily-handled bulk material with highly developed 3D porosity and excellent compressibility, which make them ideal matrix material for the support of Pd nanoparticles. The resultant Pd/GAs catalyst exhibits excellent performance for selective semi-hydrogenation reaction of phenylacetylene in terms of the activity and selectivity. Remarkably, the catalyst is recyclable for repeated use without compromise the activity and selectivity, which significantly reduce the processing cost. This work may provide new insights into the design and synthesis of recyclable and durable catalyst for a variety of applications.

Acknowledgements

This work was partly supported by Dalian S&T Program (no. 2011A15GX023), and the National Natural Science Foundation of China (no. 21003016)

References

1 C. M. Castilla and F. J. M. Hodar, *Carbon*, 2005, **43**, 455–465.
2 Z. Tang, S. Shen, J. Zhuang and X. Wang, *Angew. Chem., Int. Ed.*, 2010, **49**, 4603–4607.
3 X. Wu, T. Wen, H. Guo, S. Yang, X. Wang and A. Xu, *ACS Nano*, 2013, **7**, 3589–3597.
4 W. Cheng, C. Wang and S. Lu, *Carbon*, 2013, **54**, 291–299.
5 J. Zhang, Z. Huang, R. Lv, Q. Yang and F. Kang, *Langmuir*, 2009, **25**, 269–274.
6 X. Mi, G. Huang, W. Xie, W. Wang, Y. Liu and J. Gao, *Carbon*, 2012, **50**, 4856–4864.
7 K. S. Novoselov, A. K. Geim, S. V. Morozov, D. Jiang, Y. Zhang, S. V. Dubonos, I. V. Grigorieva and A. A. Firsov, *Science*, 2004, **306**, 666–669.
8 Y. W. Zhu, S. Murali, W. W. Cai, X. S. Li, J. W. Suk, J. R. Potts and R. S. Ruoff, *Adv. Mater.*, 2010, **22**, 3906–3924.
9 Y. Xu, K. Sheng, C. Li and G. Shi, *ACS Nano*, 2010, **4**, 4324–4330.
10 W. Chen and L. Yan, *Nanoscale*, 2011, **3**, 3132–3137.
11 H. D. Pham, V. H. Pham, T. V. Cuong, T. D. Nguyen-Phan, J. S. Chung, E. W. Shin and S. Kim, *Chem. Commun.*, 2011, **47**, 9672–9674.

12 K. W. Chen, L. B. Chen, Y. Q. Chen, H. Bai and L. Li, *J. Mater. Chem.*, 2012, **22**, 20698.
13 S. Kim, S. Lee, H. Kim, J. Hwang, W. Lee, J. Kwon, C. Bielawski and R. Ruoff, *Angew. Chem., Int. Ed.*, 2010, **49**, 10084–10088.
14 Z. Chen, W. Ren, L. Gao, B. Liu, S. Pei and H. Cheng, *Nat. Mater.*, 2011, **10**, 424–428.
15 H. Hu, Z. B. Zhao, W. B. Wan, Y. Gogotsi and J. S. Qiu, *Adv. Mater.*, 2013, **25**, 2219–2223.
16 R. V. Jagadeesh, A. Surkus, H. Junge, M. Pohl, J. Radnik, J. Rabeah, H. Huan, V. Schuenemann, A. Brueckner and M. Beller, *Science*, 2013, **342**, 1073–1076.
17 Q. M. Kainz, R. Linhardt, R. N. Grass, G. Vile, J. Perez-Ramirez, W. J. Stark and O. Reiser, *Adv. Funct. Mater.*, 2014, **24**, 2020–2027.
18 M. G. B. R. Maurer, *US Pat.* 4,822,936, 1989.
19 P. Weerachawanasak, O. Mekasuwandumrong, M. Arai, S.-I. Fujita, P. Praserthdam and J. Panpranot, *J. Catal.*, 2009, **262**, 199–205.
20 N. Xiao, Y. Zhou, Z. Ling, Z. Zhao and J. Qiu, *Carbon*, 2013, **60**, 514–522.
21 A. C. Ferrari, J. C. Meyer, V. Scardaci, C. Casiraghi, M. Lazzeri, F. Mauri, S. Piscanec, D. Jiang, K. S. Novoselov, S. Roth and A. K. Geim, *Phys. Rev. Lett.*, 2006, **97**, 187401–187404.
22 I. K. Moon, J. Lee, R. S. Ruoff and H. Lee, *Nat. Commun.*, 2010, **1**, 73–78.
23 S. Pei, J. Zhao, J. Du, W. Ren and H. Cheng, *Carbon*, 2010, **48**, 4466–4474.
24 K. Qu, L. Wu, J. Ren and X. Qu, *ACS Appl. Mater. Interfaces*, 2012, **4**, 5001–5009.
25 S. Moussa, A. R. Siamaki, B. F. Gupton and M. S. El-Shall, *ACS Catal.*, 2012, **2**, 145–154.
26 X. Mo, D. Lopez, K. Suwannakarn, Y. Liu, E. Lotero, J. Goodwinjr and C. Lu, *J. Catal.*, 2008, **254**, 332–338.